University of New Mexico
UNM Digital Repository

Chemical and Biological Engineering ETDs | Engineering ETDs

Spring 4-13-2018

An investigation of the effects of the second pyrolysis on the chemistry, morphology, and performance of iron-nicarbazin catalysts

Elizabeth B. Weiler
University of New Mexico

Follow this and additional works at: https://digitalrepository.unm.edu/cbe_etds

 Part of the Chemical Engineering Commons

Recommended Citation
Weiler, Elizabeth B.. "An investigation of the effects of the second pyrolysis on the chemistry, morphology, and performance of iron-nicarbazin catalysts." (2018). https://digitalrepository.unm.edu/cbe_etds/72

This Thesis is brought to you for free and open access by the Engineering ETDs at UNM Digital Repository. It has been accepted for inclusion in Chemical and Biological Engineering ETDs by an authorized administrator of UNM Digital Repository. For more information, please contact disc@unm.edu.

Elizabeth Weiler

Candidate

Chemical and Biological Engineering

Department

This thesis is approved, and it is acceptable in quality and form for publication:

Approved by the Thesis Committee:

Plamen Atanassov ,Chairperson

Kateryna Artyushkova

Fernando Garzon

An investigation of the effects of the second pyrolysis on the chemistry, morphology, and performance of iron-nicarbazin catalysts

by

Elizabeth B. Weiler

B.S., Bioengineering, Lehigh University, 2016

M.S., Chemical Engineering, University of New Mexico, 2018

THESIS

Submitted in Partial Fulfillment of the Requirements for the Degree of

Master of Science

Chemical Engineering

The University of New Mexico

Albuquerque, New Mexico

May, 2018

Acknowledgements

I cannot thank my advisers, Dr. Plamen Atanassov and Dr. Kateryna Artyushkova, enough for their guidance and encouragement. When I first approached them with interest in joining their research group, I thought that being a student-athlete and pursuing the thesis track for my degree would be too ambitious. While I am sure that I frustrated both of them at times with my diverted attention, their patience and supervision allowed me to accomplish the goal that brought me to Albuquerque.

I would also like to thank the cross country and track and field coaches at the University of New Mexico for welcoming me onto one of the most competitive teams in the country while also allowing me to pursue a degree with such a rigorous and demanding curriculum.

Of course, I am indebted to Dr. Kateryna Artyushkova, Dr. Michael Workman, Dr. Hien Pham, Morteza Rezaei, and Leo Chen for teaching me, more than once, every laboratory technique I used to complete this work as well as the theory behind it all.

I sincerely thank my defense committee, Drs. Plamen Atanassov, Kateryna Artyushkova, and Fernando Garzon, for their time and expertise in evaluating my work.

An investigation of the effects of the second pyrolysis on the chemistry, morphology, and performance of iron-nicarbazin catalysts

by

Elizabeth B. Weiler

B.S., Bioengineering, Lehigh University, 2016

M.S., Chemical Engineering, University of New Mexico, 2018

Abstract

Proton exchange membrane fuel cells offer a cost-effective, environmentally friendly, and sustainable alternative to petroleum-based power sources to the transportation sector. However, slow electrochemical reactions at the cathode of these fuel cell prevent the technology from being competitive. Iron-nitrogen-carbon based catalysts have emerged as a viable answer to this problem, yet further progress is needed to improve their performance beyond that of current state-of-the-art platinum-based catalysts, which are economically and geopolitically impractical to be a final solution. Currently, a two-step high temperature pyrolysis method has proven a promising way to synthesize iron-nitrogen-carbon catalysts for optimized performance, but there is a lack of general understanding as to why these techniques are so efficacious. In this study, iron-nitrogen-carbon catalysts are synthesized with varying second pyrolysis durations and analyzed in regard to their chemistry, morphology, and performance through x-ray photoelectron spectroscopy, scanning electron microscopy, and rotating ring disk electrode techniques to attempt to find trends between high performance and the occurrence of specific

chemical compositions or morphologies. It is reported that relative increases in pyridinic nitrogen and nitrogen coordinated to metal contents coincide with improved performance and that longer pyrolysis times promote heterogeneity and small scale porosity in these materials.

Table of Contents

List of Abbreviations

APXPS	Ambient Pressure X-ray Photoelectron Spectroscopy
Elements abbreviated as they appear on the periodic table, i.e. Pt denotes platinum	
Fe-NC	Iron-nitrogen-carbon based
FeNCB	Iron-nicarbazin based
FeNCB HT1	FeNCB catalyst subjected to only one pyrolysis
FeNCB HT2 5 min	FeNCB catalyst secondarily pyrolyzed for 5 minutes
FeNCB HT2 10 min	FeNCB catalyst secondarily pyrolyzed for 10 minutes
FeNCB HT2 15 min	FeNCB catalyst secondarily pyrolyzed for 15 minutes
FeNCB HT2 30 min	FeNCB catalyst secondarily pyrolyzed for 30 minutes
HT	Heat treatment (pyrolysis)
MEA	Membrane electrode assembly
NCB HT1	Nicarbazin based (metal free) sample subjected to one pyrolysis
NCB HT2	Nicarbazin based (metal free) sample subjected to a second pyrolysis of 30 minutes
Non-PGM	Non-platinum-group-metal
ORR	Oxygen reduction reaction
PCA	Principle Component Analysis
PEMFC	Proton exchange membrane fuel cell
PGM-free	Platinum-group-metal free
RDE	Rotating disk electrode
RRDE	Rotating ring disk electrode
SEM	Scanning electron microscopy
TOF	Turnover frequency
United States Department of Energy	DOE
XPS	X-ray photoelectron spectroscopy

Introduction

Section 1: Background

Last year, of the 97.4 quadrillion British thermal units (Btu) of energy consumed in the United States alone, 78 percent was sourced from fossil fuels[1]. The externalities associated with this magnitude of consumption are correspondingly enormous. In a 2005 study by the National Academy of Sciences, it was estimated that the U.S. government spent an annual $62 billion on environmental and human health damages caused by air pollution in the form of sulfur dioxide, nitrogen oxides, and particulate matter just from coal burning[2,3]. A follow-up study in 2013 not only revealed that this figure increased but that the burning of fossil fuels also contributes to four of the five leading causes of death in the United States, namely heart disease, cancer, stroke, and lung disease[2,3].

From a geopolitical perspective, the United States' reliance on foreign oil leads to rising trade deficits and controversial international agreements with unstable regions. Such consequences are exacerbated in countries with more severe international oil dependencies. A worldwide report from the International Monetary Fund, accounting for both direct costs and externalities, found global fossil fuel use costs taxpayers and consumers $5.3 trillion per year[4,5]. Yet regardless of the environmental, public health, political, and economic debates surrounding fossil fuels, the daunting yet inevitable truth remains that we are running out of our principle energy source. Some studies estimate that in as little as 50 years natural gas and oil reserves will be depleted, and coal reserve depletion could occur within 100 years[6]. In short, it is imperative that we develop reliable, clean, and renewable fuel sources in the very near future.

An immense portion of the energy flow in the United States goes to the transportation sector. In fact, only electricity generation accounts for more energy use than does transportation[1]. The overwhelming majority of this energy is derived from petroleum. Moreover, a significant percentage of the energy inputs to transportation is wasted. A 2012 summary of U.S. energy usage by Lawrence Livermore National Laboratories depicted that a mere 5.6% of the fuel put into transportation was converted into useful energy services[7]. Clearly, if a renewable, more efficient source was developed to replace the current system in transportation, an immense amount of fuel, emissions, and money could be saved.

Currently, there are multiple highly attractive solutions to the problems faced by the fossil fuel dependent transportation sector, especially regarding motor vehicles. Electric vehicles are already starting to gain ground as a market in the U.S. economy. In 2016, U.S. electric vehicle sales increased by 37 percent[8]. However, most of these commercially-available vehicles rely on battery technology. While batteries provide efficient energy storage, they require long recharging times and have relatively low energy densities[9,10]. Fuel cells overcome both of these challenges in addition to offering supplementary benefits, including reduced weight and lesser generation of greenhouse gases[9,11,12].

Although fuel cells are somewhat unfamiliar to the general public, recent advancements and simulations attest that the technology is the most promising option for replacing the internal combustion engine. A fuel cell generates electricity through chemical reactions that occur at its two electrodes, the anode and cathode. Fuel cells also require an electrolyte, which functions to transport protons and electrons between

electrodes, as well as a catalyst to increase reaction rates at the electrodes. A multitude of compounds can be used as electrolytes and catalysts, and the specific species chosen defines the type of fuel cell at work[9]. Examples of fuel cell types include alkali, molten carbonate, phosphoric acid, methanol, and solid oxide fuel cells, and there are a variety of advantages and disadvantages applicable to each form[13]. For instance, molten carbonate and solid oxide fuel cells have high efficiency ranges, but their operating temperatures are on the order of 650 to 1,000°C, making them less appropriate for use in homes and cars[10,13]. Alkali and methanol fuel cells operate at much lower temperatures; however, they involve a liquid electrolyte and fuel, respectively, leaving them susceptible to leakage, and in the case of the methanol fuel cell, the harmful greenhouse gas CO_2 is emitted[10,13]. Another kind of fuel cell, called the proton exchange membrane fuel cell (PEMFC), maintains a nearly ideal balance of the aforementioned features and has emerged at the forefront of fuel cell research[11,13].

PEMFCs exhibit an array of desirable characteristics. They employ a permeable solid polymer electrolyte whose flexibility resists leaking and cracking. Due to relatively low operating temperatures under 100°C, PEMFCs have faster start times and better durability than some other fuel cell types[11]. However, one of the most significant drawbacks to PEMFC technology is slow electrochemical reactions at the cathode, which result in huge potential losses and excessive heat generation[11,14]. If solutions to this problem could be discovered to improve the efficiency of these fuel cells, then PEMFCs would prove to be a relevant competitor to traditional energy systems.

For reactions of biologic and synthetic nature alike, the optimal way of increasing reaction rates is to incorporate an appropriate catalyst into the system. This holds true for

the electrochemical oxygen reduction reaction (ORR) that occurs at the cathode of PEMFCs. Today's state-of-the-art catalysts for PEMFC cathodes are platinum (Pt) based. While such systems show impressive durability and supply enough power to compete with internal combustion engines, the material they require is extremely costly. Pt prices are largely unstable, fluctuating around $1,000 per ounce[15]. To reduce costs, many researchers have focused their efforts to developing fuel cells that can operate with ultra-low Pt loading. This approach has indeed shown some success; however, even if this technology continues its impressive progress, Pt catalysts will still face geopolitical challenges. Some studies estimate that as much as 90% of the known Pt supply comes from South Africa and Russia alone[16]. Given the long history of international conflict fueled by dependence on foreign oil[17–19], the introduction of a fuel economy with a principle resource once again confined to isolated geographical regions is far from ideal. Therefore, it is highly desirable to employ ORR catalysts that are not at all Pt-based.

In the mid-1960s, non-precious-metal-based ORR catalysts of very modest performance began to emerge for PEMFC cathodes[20]. This class of catalysts is generally referred to as non-platinum-group-metal (non-PGM) or platinum-group-metal-free (PGM-free) catalysts. The breakthrough for non-PGM catalysts occurred when researchers were inspired by biological enzymes that reduce oxygen for cellular respiration purposes in prokaryotes and mitochondria[16,20,21]. By mimicking the enzymes' heme-copper active site, it was found that Fe coordinated to phthalocyanine could efficiently catalyze oxygen reduction on an electrode surface[21]. As further progress in the field has been made, catalysts that incorporate either the Fe or Co transition metal with nitrogen and carbon species prove to be the best candidates for replacing Pt-based

catalysts[16]. Iron-nitrogen-carbon (Fe-NC) based electrocatalysts show particular promise as many exhibit high ORR activity in both acidic and alkaline media as well as impressive durability and membrane electrode assembly (MEA) performance[22]. These three characteristics are not only critically important for satisfying the DOE volumetric activity and operation hours targets but also for addressing the greatest barriers PEMFCs with non-PGM cathode catalysts face for commercialization.

For non-PGM catalysts to emerge as the decisively superior alternative to Pt-based catalysts, they must obviously match or exceed the ORR activity values established by Pt. Significant advancement has already been made here, as the materials needed for non-PGM catalysts synthesis are both abundant and inexpensive, which allows for much higher loadings than those viable for Pt[10]. However, higher loadings equate to increased thickness of the catalyst layer. Since thicker catalyst layers hinder mass transport, non-PGM electrocatalyst site density tends to be lower than that of PGM catalysts[10,23]. This problem highlights the importance of catalyst durability (the duration for which a catalyst can sustain a minimum level of performance). If non-PGM catalysts inherently have lesser initial performance than Pt catalysts, then they must demonstrate minimal performance loss over time relative to Pt. Indeed, several research groups at the forefront of the non-PGM catalyst field have proven that through the employment of Fe-NC based catalysts, it is possible to address these concerns.

Over the last few years, an abundance of literature has arisen to evidence the potential of Fe-NC based catalysts for oxygen reduction. For example, in 2011 Eric Proietti, et al demonstrated that a cathode with a Fe-phenanthroline-Zn(II) zeolitic imidazolate catalyst delivered comparable power density to that of a state-of-the-art Pt

cathode[16]. Power density is an immensely important metric for fuel cell performance as it reflects the time rate of energy transfer that can be supplied per unit volume[24]. Figures 1a and 1b below depicts the comparison of power density among the study's two iron-based catalysts and Pt catalyst as well as a comparison of each cathodic systems' polarization curves. Polarization curves represent another useful measure in the field of fuel cell catalysis as they reveal the relationship between electrode potential and current density, which is indicative of the maximum power density that can be achieved[25].

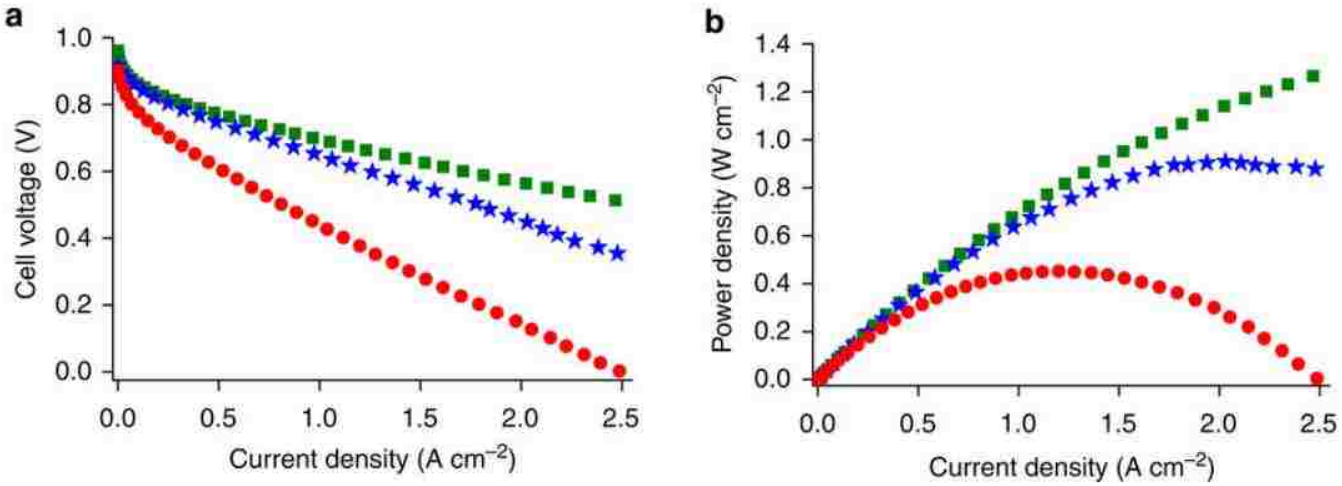

Figure 1[16]**: (a)** Polarization curves for three MEAs of three different cathodic materials. The green squares represent the polarization curve of the Pt-based cathode, the blue stars represent the polarization curve of the researchers' best performing Fe-phenanthroline-Zn(II) zeolitic imidazolate catalyst at the MEA cathode, and the red circles represent the polarization curve for the cathode with a different iron-based catalyst previously synthesized by the same researchers. **(b)** Power density curves for the same respective MEAs.

As clearly seen above, the activity of the Fe-phenanthroline-Zn(II) zeolitic imidazolate catalyst is highly competitive with that of the Pt catalyst. Other groups of investigators have synthesized Fe-NC catalysts of different formulations and have not only seen similar trends in activity but also in respect to durability. In 2015, researchers at the University of New Mexico found that electrocatalysts made from precursors of iron

nitrate and a nitrogen-containing charge-transfer salt known as nicarbazin showed both high activity and durability. This was accomplished through a basic technique frequently used in electrochemical reaction studies: rotating ring disk electrode (RDE). The experimental setup for RDE involves a few essential components. A working electrode acts as the surface at which an electrochemical reaction of interest takes place[26]. Because of this, the working electrode is generally the surface at which a catalyst is deposited, as was done in the study of the iron-nicarbazin catalyst at the University of New Mexico. There is also the reference electrode, which serves as a reference to which the potential of the working electrode is measured. The reference electrode has a stable and well-known potential to ensure a controlled and reliable experiment[26]. The electrical circuit is completed via the counter electrode, occasionally referred to as the auxiliary electrode, and is also the point through which a current is injected to the electrochemical cell[26]. Therefore, the counter electrode must be an inert conductor, like platinum or graphite. Finally, RDE experiments require a potentiostat for controlling the voltage difference between the working and reference electrodes[26]. All these components render RDE a quick and efficient method for studying redox chemistry, especially the half reaction that occurs at fuel cell cathodes: oxygen reduction. When an additional electrode in the form of a ring around the original working disk electrode is added to the experimental scheme, the other half reaction can be studied. This technique, known as rotating ring disk electrode (RRDE) is equally important for evaluating ORR catalysts as the half reaction that occurs at the ring electrode involves hydrogen peroxide generation, which is ideally minimized when a good catalyst is employed. Figure 2 below illustrates the results of the RDE experiment that employed the iron-nicarbazin (FeNCB) catalyst.

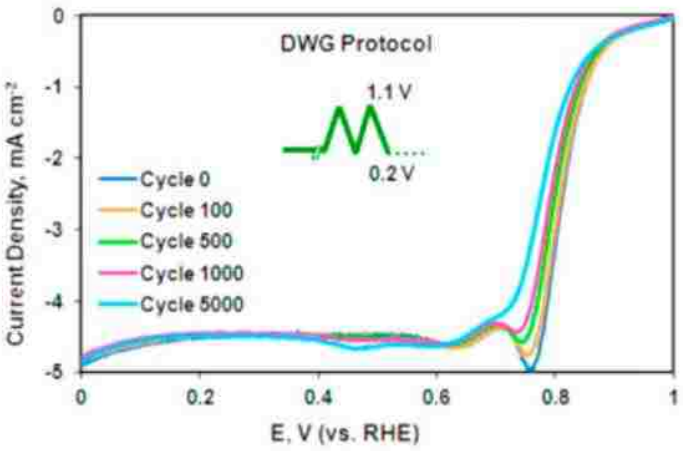

Figure 2[27]: Voltammogram of RDE experiment with the FeNCB catalyst at the working electrode surface.

Here, the FeNCB catalyst exhibits consistent performance after thousands of RDE voltammetry cycles performed in accordance with the DOE's Durability Working Group (DWG) protocol, which specifies the recommended conditions under which the voltammetry experiments should be performed so the technique may act as a screening test for catalysts that may show promising activity for fuel cell appliciation[28]. In fact, this FeNCB catalyst performed so well that it has remained an ongoing focus of the research team's efforts to bring non-PGM materials to the forefront of PEMFC catalysis. Yet an enormous challenge must be addressed. Before FeNCB catalysts, or any other Fe-NC based catalysts, can advance to practical application, the mechanisms that make these materials good catalysts must be elucidated. Without a more complete understanding of the reason behind the impressive performance of FeNCB catalysts, any attempt to alter their properties for improvement will be nothing more than blind trial and error.

Section 2: Literature review and need for research

The best performing Fe-NC catalysts, despite varying formulations, do share some common features, particularly in how they are synthesized. After the initial mixing

of iron, nitrogen, and carbon sources, the materials are frequently subjected to heat treatment, or pyrolysis, in a tightly controlled atmosphere. Recent publications have begun to outline how these synthesis specifications correlate to catalyst properties. For example, in 2016 academics in China showed that when heat treated Fe-NC materials were subjected to ball-milling, a process in which powders are ground at high rotation speeds to promote homogeneity of the material, and a second pyrolysis, the resultant catalysts exhibited much higher activity than those synthesized from a one-step pyrolysis[29]. In 2014, a different group of Chinese scientists found that Fe-NC catalysts pyrolyzed at higher temperatures, about 950^{o}C, attained higher activity than those pyrolyzed at lower temperatures[30]. Another study published by researchers at the Helmholtz-Center Berlin for Materials and Energy demonstrated that Fe-NC catalysts exhibited substantially higher ORR activity when ammonia was employed as the gas to control atmospheric conditions during the second pyrolysis[31]. One of the most comprehensive studies of Fe-NC catalyst synthesis effects came from the dissertation work of Dr. Michael Workman at the University of New Mexico, the same group which produced the well-performing and highly durable FeNCB catalyst discussed above. In one of his studies published last year, Workman et al varied numerous synthesis parameters, including those investigated in the other studies referenced in this section, and used RDE, MEA, and x-ray photoelectron spectroscopy (XPS) techniques to evaluate how the synthesis variations correlated with the performance and structural properties of the catalyst[32]. XPS, a technique in which x-rays irradiate the surface of a material and the kinetic energy of escaping electrons is measured to identify elemental composition, has proved invaluable in the study of Fe-NC catalysts as its detection limits allow for detailed

study of the nitrogen and carbon species of the materials[10]. The results of Workman's study corroborated much of what had been previously suggested on the subject. For example, it was confirmed that subjecting the FeNCB precursors to an initial high temperature pyrolysis, subsequent ball-milling, and then to a second high temperature pyrolysis under ammonia led to higher activity. It also introduced new postulations about what increases catalyst activity by proposing the composition of the catalysts' active sites. The group's results indicated that the presence of Fe nanoparticles reduced activity and highlighted the importance of incorporating acid leeching into the synthesis process to reduce these phases[32]. In doing so, it was noted that the relative amount of atomically dispersed Fe and nitrogen-iron species increased[32]. When such increases occurred, catalyst ORR activity also increased, indicating these sites in which nitrogen an iron are coordinated serve as the active sites. Yet an even more surprising phenomenon was observed. Any synthesis alterations made following the first pyrolysis seemed to affect the final catalyst activity most drastically. The authors note in their conclusion that "the significant influence of treatments following the first pyrolysis suggests that the active sites are either fragile and easily destroyed before the second pyrolysis or, more likely, that they are primarily created during the second pyrolysis"[32]. Such a statement demands more research into the role the second pyrolysis plays in determining the properties of FeNCB catalysts. If this need were met, then the current understanding of what can be done to produce an efficient non-PGM catalyst could be expanded and more informed and direct action could be taken to synthesize such materials.

Although efforts to address this need have been made, the vast majority of research that has been done to investigate the relationship between the second pyrolysis

and Fe-NC catalyst properties emphasize one theme: how optimization of second pyrolysis specifications leads to a greater presence of iron-nitrogen coordinated species that most likely serve as active site, which in turn improves catalyst activity. In many ways, the studies I have already mentioned fit this mold. For instance, the study of the Helmholtz-Center Berlin found that a second pyrolysis performed under ammonia gas seemed to increase the turnover frequency of FeN_4 centers while catalyst activity also increased, indicating the potential for FeN_4 species as active sites[31]. Turnover frequency (TOF) refers to the number of moles of reactants a catalyst transforms into the desired product per number of active centers or surface area per unit time and is a common metric for activity level. A similar study published in the same year by Juan Herranz et al substantiated these findings surrounding FeN_4 sites[33]. Other works have made novel contribution by specifically focusing on secondary pyrolysis chemistry of nitrogen functional groups. As illustrated in Figure 3a, b, c, and d below, a publication by Gang Liu, et al revealed that catalyst stability could be enhanced by increasing the content of quaternary nitrogen groups in their Fe-NC catalyst[33].

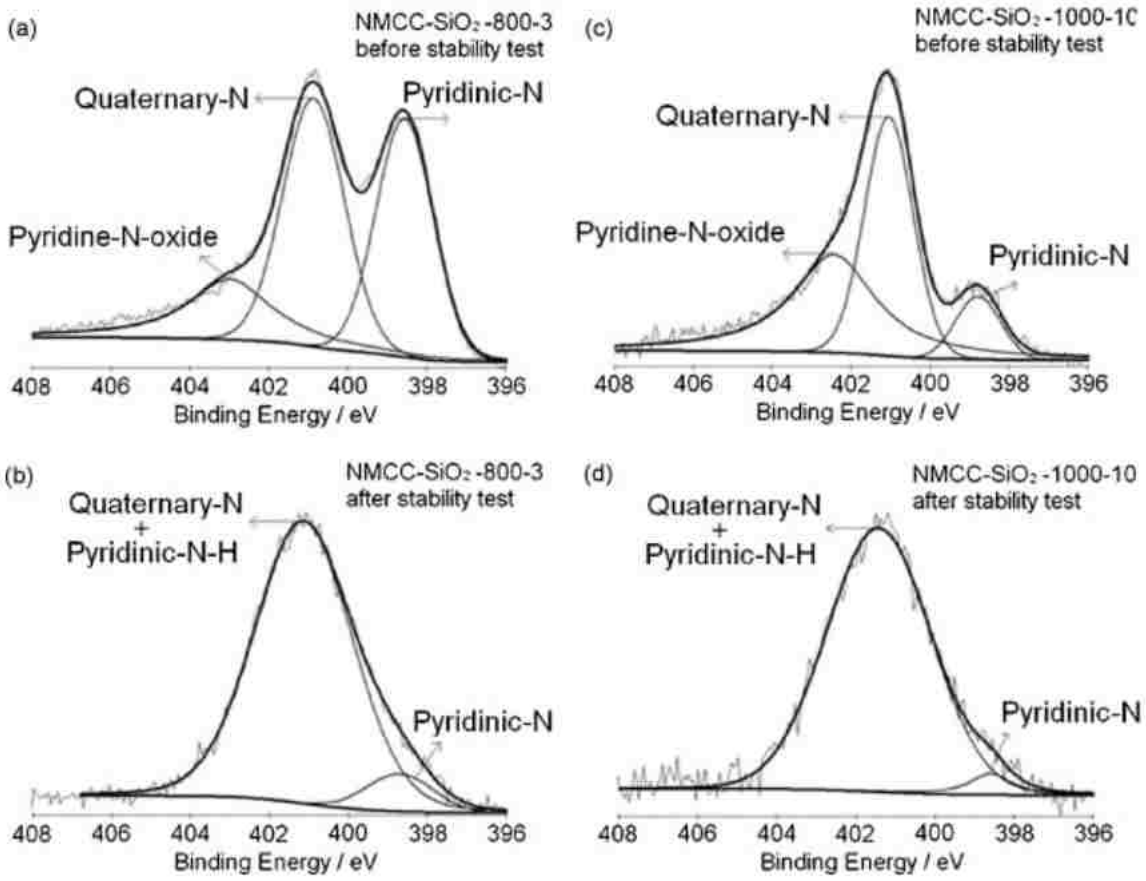

Figure 3[33]: XPS results from Gang Liu, et al. (a) and (c) show XPS results of two different Fe-NC catalysts before the stability test was performed (the NMCC abbreviations designate how the group named their Fe-NC catalysts). (b) and (d) show XPS results of the same respective samples after they were put through the stability test.

Through this illustration, we can see that while some nitrogen species significantly degraded after the stability test was performed, the quaternary-nitrogen groups remained intact, indicating that it is these sites that have the greatest stability and therefore may contribute to the stability of the catalyst. While publications like this have invaluably built upon the story of the chemistry behind the second pyrolysis of Fe-NC catalysts, all have relied upon analyses performed after total completion of the second pyrolysis. If data could be collected from earlier stages of the second pyrolysis, then this story could be much more complete. The aim of my work herein will attempt to do just this.

Section 3: Objective of study

This study has two key goals. The first is to determine how the chemistry and morphology of FeNCB catalysts change over the time of the second pyrolysis. In respect to chemistry, the evolution of nitrogen species is especially focused on since nitrogen functional groups have been previously flagged as important components of Fe-NC catalyst active sites[34,35]. To accomplish this, FeNCB samples with varying times of exposure to second pyrolysis conditions are synthesized and analyzed via XPS and Ambient Pressure XPS to evaluate chemical changes, while scanning electron microscopy is employed to study morphological change.

The second objective of this work is to correlate catalyst composition and performance via a comparison of XPS and Ambient Pressure XPS data and RRDE performance data.

Materials and Methods

Section 1: Synthesis

Overall, the procedure for the synthesis of all samples closely followed that of the sacrificial support method using iron and nicarbazin precursors as described previously in multiple works published by my research group[10,27,32]. A calculated ratio of nicarbazin (1,3-bis(4 nitrophenyl)urea; 4,6-dimethyl-1H-pyrimidin-2-one, Sigma-Aldrich), silicas (Cab-O-Sil® LM-150 fumed silica, Cab-O-Sil OX-50 fumed silica, and house synthesized 370 nm Stöber spheres), and iron (III) nitrate nonahydrate ($Fe(NO_3)_3 \cdot 9H_2O$) were mixed together with distilled water in a beaker, sonicated for 30 minutes, and then placed with a stir bar on a heated stir plate at 45°C overnight. The following day the

precursors were moved to a 45ºC drying oven and left to dry overnight. Next, the material was broken up using a mortar and pestle and ground to a coarse powder. The material was then ground to a fine powder using an agate ball mill jar and ball mill. Subsequently, a heat treatment (HT) was performed on the material by means of a tube furnace. The quartz tube containing the material maintained a controlled atmosphere of 7% H_2: 93% N_2 at a flow rate of 120 standard cm^3 min^{-1} and was placed into the furnace at 525ºC where the set temperature was then immediately turned to 900ºC. As the furnace reached 900ºC, the temperature was increased to 975 °C at a rate of 10 °C min^{-1}. The material was subjected to a constant 975ºC temperature for 45 minutes. The tube was then removed from the furnace to quench the material. Once all the precursor material was heat treated in this way, it was ball milled in an agate jar for one hour. The heat treated powder was then placed into a solution of 20 mL distilled water where 35 mL 49% hydrofluoric acid were then gradually added. After one full day of acid leaching, an additional 15 mL 49% hydrofluoric acid were added. After two more days, for a total of four days of leaching, the material was washed distilled water until a pH greater than 5 was attained. A vacuum flask was used to filter the catalyst from the water, and the powder was then placed in a 85ºC drying oven overnight. Next, a second HT (HT2) was performed again using a tube furnace. A flow rate of 120 standard cm^3 min^{-1} of 10% NH_3: 90% N_2 was maintained and the temperature was held at 950ºC. The duration of the HT2 is what differentiated each of the five FeNCB samples in this study. One sample was not subjected to a second heat treatment at all and served as the “time zero” sample. The remaining four samples were synthesized by taking a portion of the HT1 sample and performing the HT2 for 5, 10, 15, or 30 minutes for the respective sample. The time of

HT2 refers to the number of minutes the samples was exposed to the conditions of the HT2 after the tube was put into the furnace and the furnace returned to the set temperature of 950^{o}C. A HT longer than 30 minutes was not performed as our group has previously demonstrated than a HT2 exceeding 30 minutes does not improve or hinder catalyst performance. After each sample was subjected to its designated HT2, it was ball milled in an agate jar for 1 hour. Two batches of all samples were synthesized and analyzed separately to examine reproducibility.

The two metal-free samples in this study were synthesized according to the procedure above; however, no iron (III) nitrate nonahydrate was added to the initial mixture. Only a HT1 and HT2 sample were prepared and analyzed.

Section 2: XPS

All XPS spectra associated with this study were acquired on a Kratos Axis Ultra X-ray photoelectron spectrometer equipped with a monochromated Al Kα X-ray source operating at 300 W. Three regions were analyzed per sample without charge neutralization. CasaXPS software was utilized for both data analysis and quantification.

Section 3: Ambient Pressure XPS (APXPS)

APXPS was employed in this study as its synchrotron sources allow for greater precision in analyzing the outermost surface layers of a material as well as its chemical composition upon exposure to the atmosphere[34]. All APXPS spectra were acquired at the Innovative Station for In Situ Spectroscopy at Helmholtz-Zentrum Berlin with calibration and operating parameters previously used for similar analysis of FeNCB and NCB materials by our group[34].

Section 4: Scanning electron microscopy (SEM)

A Hitachi S-800 instrument was used to acquire all images. 6 different regions on each sample were imaged, and the extracted parameters were averaged to obtain final values. All error bars in figures are representative of the standard deviation between the 6 different values obtained for each sample. To discourage confusion between sample variations due to differences in morphology versus instrumental influences, all images were acquired at 2kV voltage and 50k magnification[36]. Analysis of all SEM images was done through Digital Image Processing via a Matlab program written by Dr. Kateryna Artyushkova[37].

Section 5: Rotating Ring Disk Electrode

RRDE measurements were performed using Pine Research instrumentation. The experimental setup for tests of all samples included a glassy carbon working electrode with disk area 0.2472 cm^2, a graphite counter electrode, and a Ag/AgCl reference electrode. In addition, an O_2 saturated 0.5 M H_2SO_4 solution at room temperature served as the electrolyte. Ink composition consisted of 5 mg catalyst from the respective sample, 925 μL 4:1 isopropanol: distilled water, and 75 μL 1.0 wt. % Nafion solution. After the initial mixing of the three materials, inks were sonicated for a total of 90 seconds. Inks were deposited onto the electrode surface for a total catalyst loading of 600 $\mu g/cm^2$. AfterMath software was employed to control experiment parameters and set a rotation speed of 1600 rpm and sweep rate of 5 mv s^{-1}. As all measurements were taken vs. a saturated Ag/AgCl reference electrode, data was transformed to reversible hydrogen

electrode potentials via the addition of 0.215 V. Half-wave potentials were determined through calculation of the second derivative of the disk current density sigmoid.

Results and Discussion

Section 1: APXPS and XPS data from first batch of samples

APXPS is a highly attractive technique in materials science studies as it allows for real-time investigation of solid surfaces in the presence of a gas or vapor phase[38]. Since a fuel cell environment consists of both oxygen gas and water vapor, APXPS provided valuable insight into the evolution of the chemistry of FeNCB catalysts and metal-free analogs during the second pyrolysis. Figure 4 below shows a comparison of high resolution N 1s spectra before and after second pyrolysis treatment in both FeNCB and metal-free samples. Nitrogen analysis was emphasized not only because nitrogen species are thought to be centers for active sites in Fe-NC catalysts, but also because nitrogen photoelectrons have a high signal-to-noise ratio and are very sensitive to binding energy shifts, which allow for more acute detection in chemical changes[34].

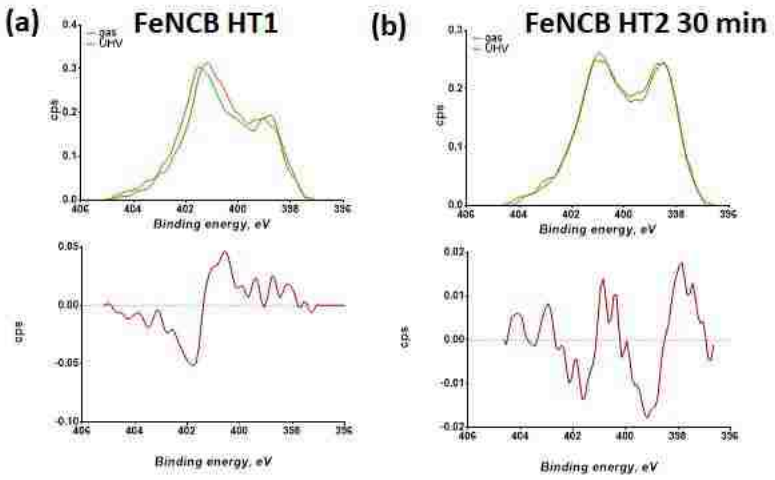

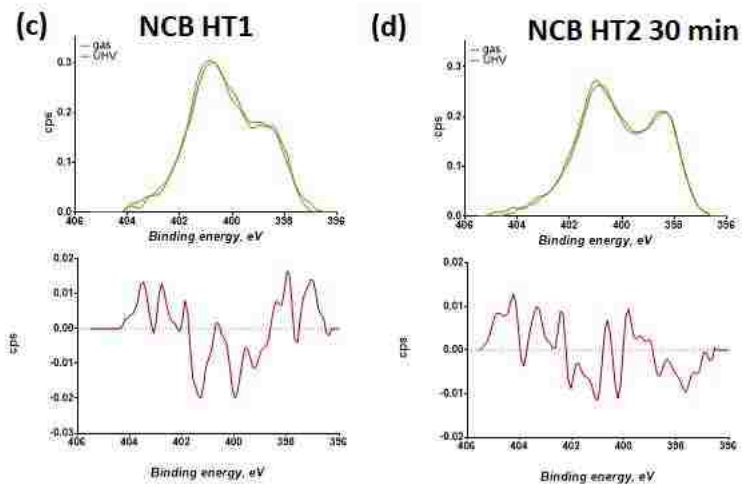

Figure 4: High resolution APXPS spectra for N 1s under O_2/H_2O (orange, pressure of 0.5 mbar) and ultrahigh vacuum (UHV) (green, pressure of $2 \cdot 10^{-9}$ mbar) conditions.

In Figure 4a, the most prominent feature is the large peak between 400 and 402 electron volts (eV), which corresponds to oxygen bound to pyrrolic nitrogen[39]. But in Figure 4b, another large peak has formed around 398 eV, indicating more pyridinic binding after the second pyrolysis[39]. The other major difference between the spectra shown in figure a and b is the significant signal increase between 398 and 400 eV, which is suggestive of nitrogen bound to metal[39]. This makes sense when all spectra in Figure 4 are considered. In Figure 4c and 4d, a similar trend can be seen in respect to pyrrolic and pyridinic nitrogen binding. But as signified by the spectra in red, any binding phenomena that is occurring in the metal free (NCB) samples is well below the statistical significance of noise, while major shifts are occurring in the FeNCB samples giving further evidence for iron nitrogen binding. Figure 5 below more explicitly illustrates these changes in the FeNCB samples.

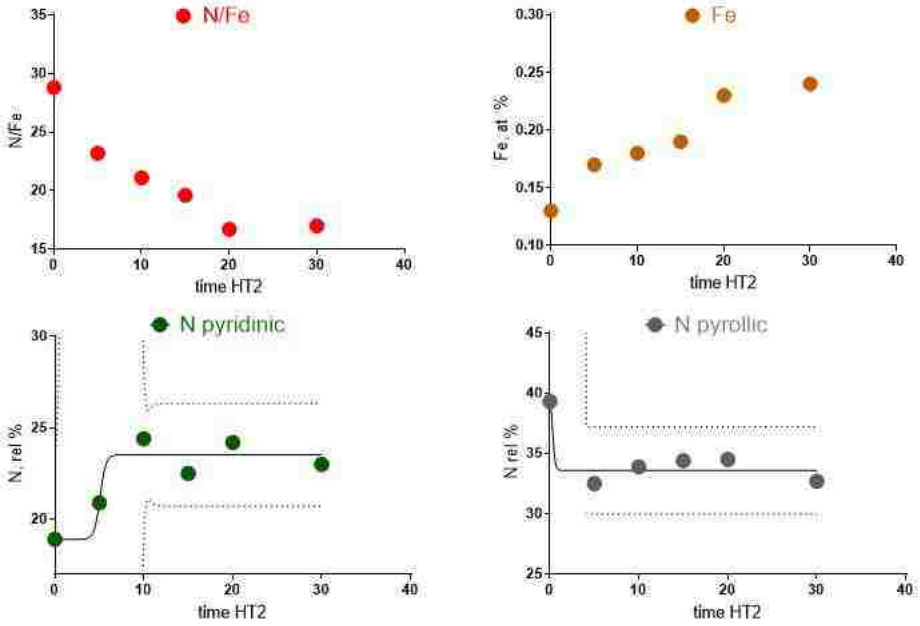

Figure 5: Compositional XPS data for FeNCB samples.

As suggested by the APXPS spectra, compositional data from XPS confirms that the relative amount of pyrollic nitrogen decreases while the amount of pyridinic nitrogen increases. It is also seen that the ratio of nitrogen to iron decreases over the course of the second pyrolysis. While this probably is simply because the atomic percentage of iron increases, it is interesting that such changes occur even as the pyrrolic and pyridinic nitrogen chemistries seem to be stabilizing. Looking more closely at this stabilization, the respective decrease and increase in pyrrolic and pyridinic nitrogen species primarily happens within the first five minutes of the second pyrolysis. Similar trends in morphological changes of the FeNCB samples are presented next.

Section 2: SEM results

The data shown in this section was obtained through the evaluation of statistical parameters extracted from the images of the samples. This was accomplished through the

employment of a multivariate statistical method of data analysis known as Principal Component Analysis (PCA). The theory and applications behind the technique have been detailed in previous publications[36]. While this method allows for the extraction of over 15 parameters per sample, only 4 proved are presented in this work as these proved to be the only parameters that showed statistical significance and consistent trends. Figure 6 below shows the trends observed for both uniformity and entropy as a function of the time of the second pyrolysis. In the case of PCA of SEM images, uniformity refers to the measure of the occurrence of ideal repetitive structures, while the term entropy refers to the measure of the degree of randomness based on the average uncertainty of grey tone co-occurrence in the image. In other words, uniformity is a measure of sample homogeneity, and entropy is a measure of sample heterogeneity.

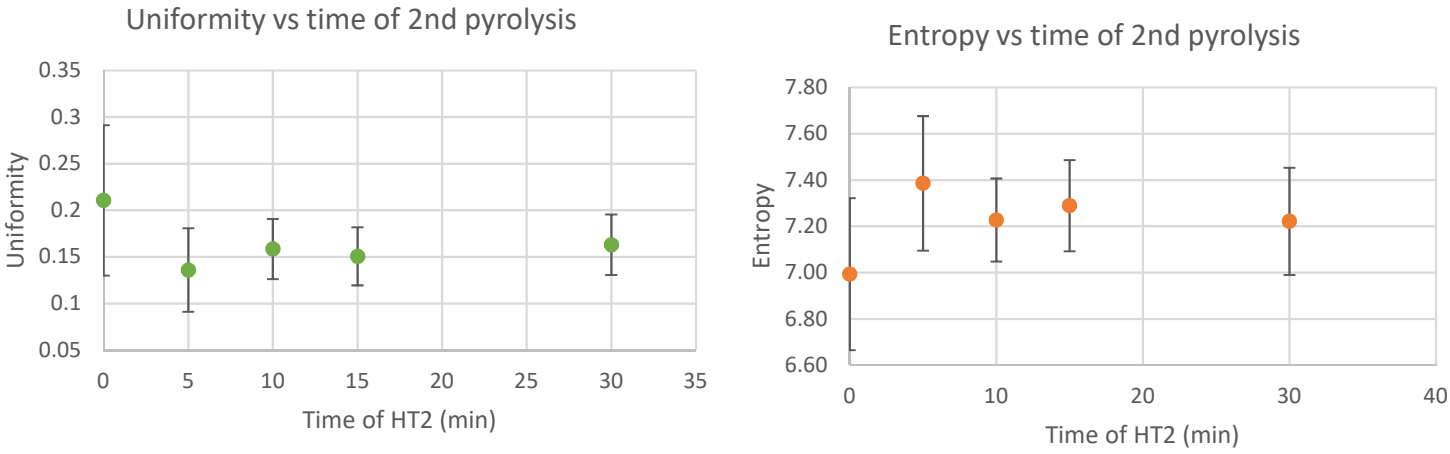

Figure 6: (left) PCA uniformity values for FeNCB samples (right) PCA entropy values for FeNCB samples

Intuitively, these parameters show opposite trends. Within the first five minutes of the second pyrolysis, the uniformity, or homogeneity, of the material decreases, while the entropy, or heterogeneity of the material is increases.

The other two statistical parameters of relevance in this study are roughness parameters. One is small scale porosity (RskH), which is a term for the skewness of the image and is measured by the asymmetry of the roughness profile. "Small scale" refers to a region size of 9 to 40 pixels on the image. The final statistical parameter evaluated was large scale porosity (RskL). This parameter is measured in the same way as RskH, except for a range of 200 to 300 pixels. The trends for small scale porosity and large scale porosity are illustrated in Figure 7 below. For PCA, a lesser statistic equates to a greater number of pores.

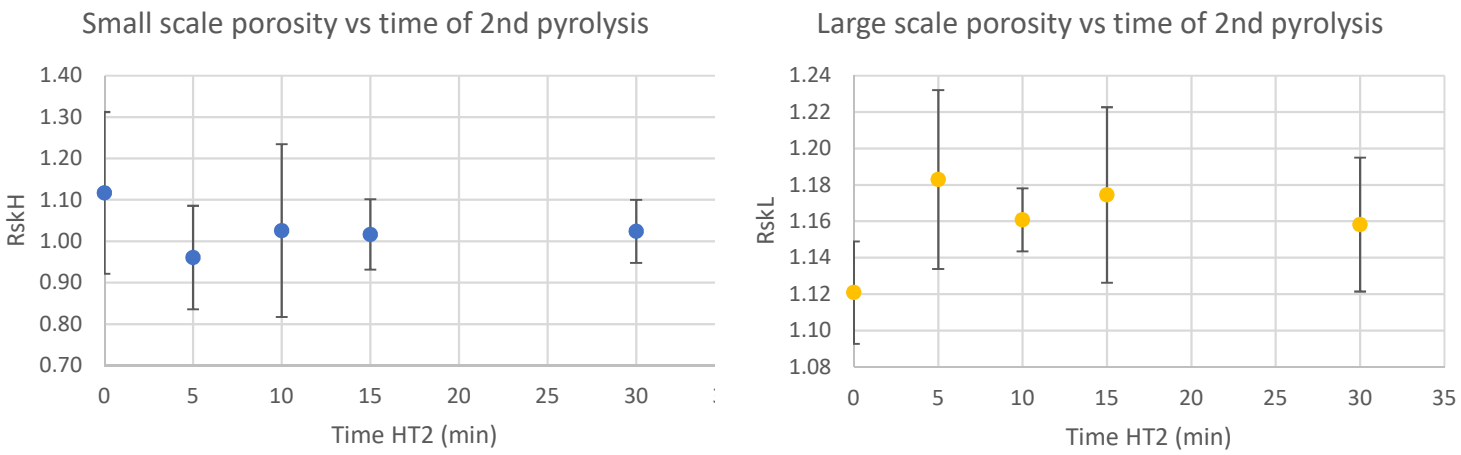

Figure 7: (left) changes in small scale porosity of FeNCB samples (right) changes in large scale porosity for FeNCB samples

Since both the RskH and RskL parameters are inversely proportional to the quantity of pores, it can be seen that the number of small pores in the material increases with time of the second pyrolysis, while the number of large pores decreases. For a better understanding of what constitutes "small" and "large" pores, mathematical equations have been established to relate the number of pixels comprising a region of a SEM image to physical dimensions through the total number of pixels in the field of view of the image[10,36]. In this case, the 9 to 40 pixel range of small scale pores corresponds to a

physical pore size between 18 and 80 nanometers, and the 200 to 300 pixel range of large scale pores corresponds to pores between 400 and 600 nanometers.

In the examination of both heterogeneity and porosity as functions of time of the second pyrolysis, the most significant changes occur within the first five minutes of the second pyrolysis, in which overall heterogeneity increases and the number of pores ranging from 18 to 80 nanometers in size increases while the number of pores from 400 to 600 nanometers in size decreases. This result indicates that the first few minutes of the second pyrolysis are critical for the overall morphology of the catalyst. However, in the case of the porosity trends the standard deviation among measurements was quite large, so these findings may hold less significance.

Section 3: RRDE data from first batch of FeNCB samples

For all RRDE experiments in this study, the standard in assessing catalyst performance was the half-wave potential, which was obtained from the second derivative of the disk current density sigmoid as a function of the corrected potential. A larger half-wave potential value is indicative of better performance. A comparison of the disk current density curves of each sample is illustrated below along with Table 1 summarizing the half-wave potentials ($E_{1/2}$) calculated from each curve. The $E_{1/2}$ values spanned 725 mV to 755 mV vs RHE with the HT2 5 min sample performing the worst, and the HT2 30 min sample performing best.

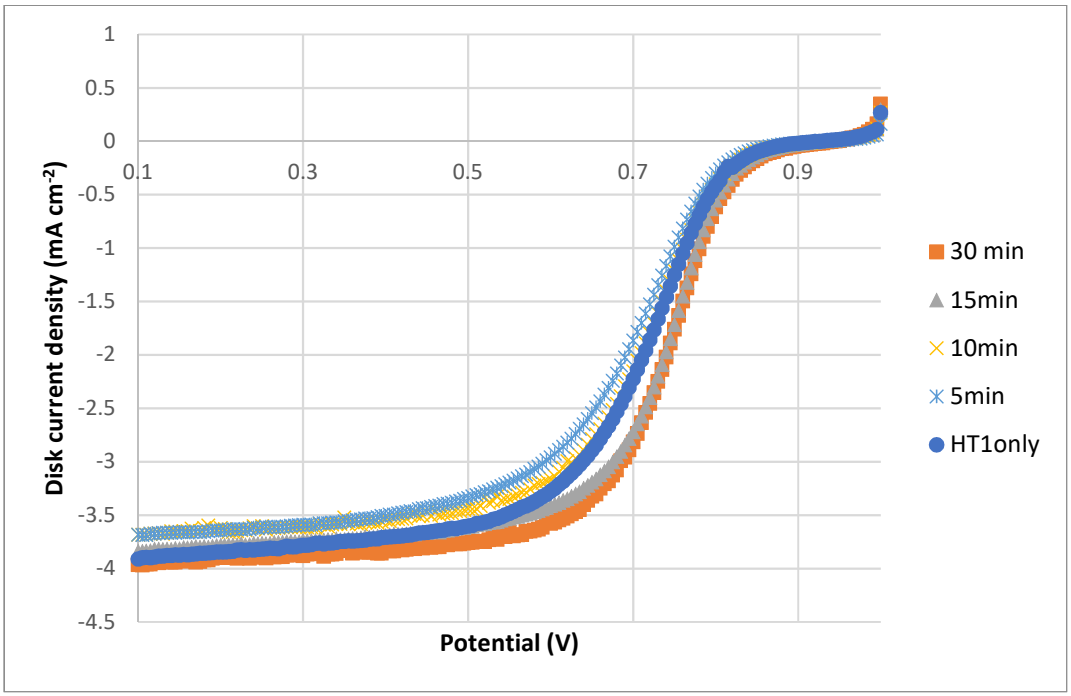

Figure 8: Disk current density vs potential curves for five samples of varying second pyrolysis durations. RRDE experiments were performed in 0.5 M H_2SO_4 at 5 mV s^{-1}.

Sample	$E_{1/2}$ (mV)
HT1	745
HT2 5 min	725
HT2 10 min	730
HT2 15 min	755
HT2 30 min	755

Table 1: Summary of the half-wave potentials vs RHE calculated for each sample.

Here it is observed that during the first five minutes of the second pyrolysis, performance actually decreases, and it is not until a sample is exposed to the second pyrolysis conditions for 15 minutes that the performance surpasses its initial value. A more detailed analysis of these results is given in the discussion of the RRDE results of the second batch of catalysts due to reproducibility issues that must be addressed.

Given the capabilities of RRDE, performance was not the sole feature investigated using this technique. Indeed, RRDE is valuable for evaluating other phenomena related to the activity of ORR catalysts. For example, electron transfer has significant implications in how well a catalyst can be said to perform as the ORR can proceed via two different pathways. First, in a two-electron pathway, oxygen can react to form a hydrogen peroxide intermediate. This intermediate then reacts with two protons and two more electrons to form water. Alternatively, oxygen can react to form water directly in a four-electron transfer. The latter pathway is much more favorable in fuel cell applications, as hydrogen peroxide is detrimental to the cell environment. Therefore, catalysts that encourage direct four electron transfer are far more promising for PEMFC application. Quantifying electron transfer in RRDE experimentation is well established and can be done by applying the following equation:

$$\#\ electrons = \frac{4I_d}{(I_d + \frac{I_r}{e})}$$

where I_d represents disk current density, I_r represents ring current density, and e is the collection coefficient, the value of which is provided by the RRDE equipment manufacturer. Figure 9 exemplifies how this quantification was applied in this experiment.

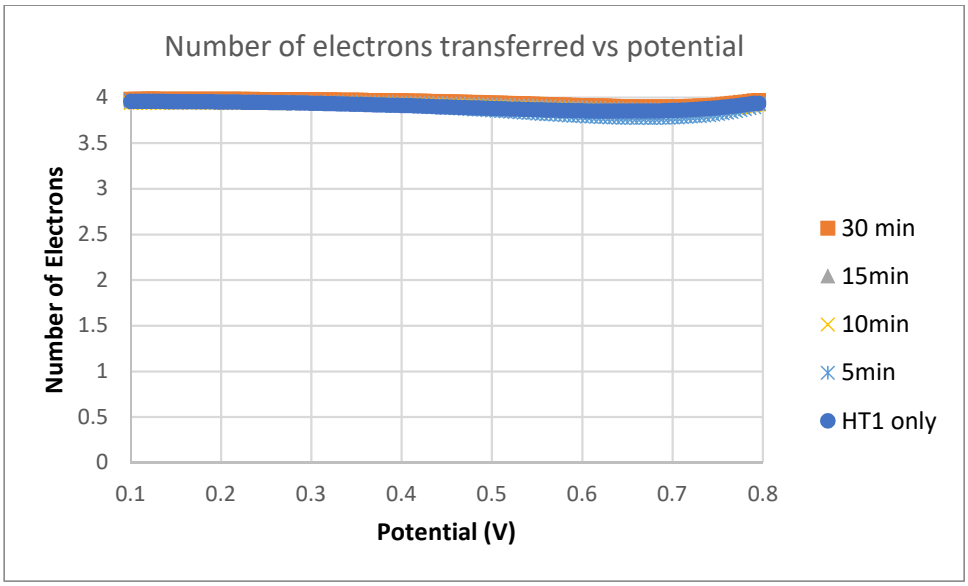

Figure 9: Trends in the number of electrons transfer in the ORR half reaction among FeNCB samples

For all samples, the overwhelming majority of reaction pathways that occurred followed a four-electron transfer, indicating a FeNCB catalyst subjected to any stage of the second pyrolysis performs desirably in regard to electron transfer.

Another important analysis to consider is that of peroxide yield. As mentioned above, it is vital to avoid hydrogen peroxide generation during fuel cell operation. The quantification of peroxide yield is similar to that of electron transfer in that it involves a simple equation with nearly identical variables:

$$Hydrogen\ Peroxide\ yeild = \frac{(\frac{2I_r}{e})}{(I_d + \frac{I_r}{e})} \times 100\%$$

again, where I_r represents ring current density, I_d represents disk current density, and e represents the collection coefficient. The results of this experiment's hydrogen peroxide generation are shown below.

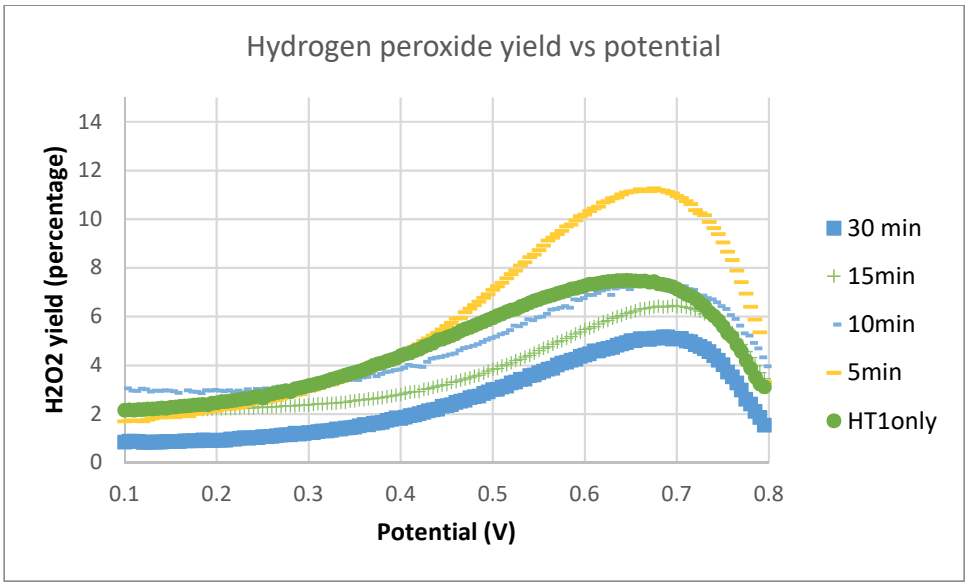

Figure 10: Levels of hydrogen peroxide yielded in the activity of FeNCB samples

The trend seen here closely follows that observed for the $E_{1/2}$ values of the sample set. Overall, all the samples exhibit respectable performance in terms of minimizing hydrogen peroxide generation as the yield never exceeds a value of about 12%. But as seen with $E_{1/2}$ results, the HT2 5 min sample performs the worst as it generates the greatest percentage of hydrogen peroxide, while the HT2 30 min sample performs best as it generates the lowest percentage of hydrogen peroxide. Also, it is not until the HT2 15 min that the hydrogen peroxide generation is reduced to a level below that of the sample that subjected to only one pyrolysis.

The findings of this section can be summarized as follows:

1. Catalyst $E_{1/2}$ values ranged from 725 mv to 755 mV. The HT2 5 min sample showed the lowest performance, while the HT2 15 min and HT2 30 min samples performed best as both reached $E_{1/2}$ values of 755 mV,

proving they are highly competitive with state-of-the-art Pt catalysts for ORR activity[40].

2. All catalysts predominately exhibited desirable four-electron transfer.
3. Similar trends were observed among sample performance with regard to $E_{1/2}$ and hydrogen peroxide yield. In both cases, performance initially decreased from activity values attained after just one pyrolysis was performed, and it was only the performance of HT2 15 min and HT2 30 min samples that surpassed these initial values.

In the next section, I present the RRDE results of a subsequently synthesized batch of FeNCB catalysts to emphasize how batch-to-batch variability carries significant implications in how these trends can be interpreted.

Section 4: RRDE data from second batch of FeNCB samples

After an identical synthesis of all five FeNCB samples was completed, an identical RRDE experiment to that outlined in the previous section was performed to evaluate reproducibility. Overall, there was great difficulty reproducing the trends previously observed; however, such problems are not unfamiliar to this field and have been well documented in the literature[41,42]. Even when catalyst loading held constant, deposition onto the electrode is not fully controllable, resulting in variable catalyst distributions on the electrode. It is also been suggested that hydrogen peroxide can distort instrument signaling when it is transported to the surface of the reference or counter electrodes[41]. These factors not only affect batch-to-batch performance variability but also cause performance variability for a single sample. For example, RRDE experiments from the first batch of FeNCB catalysts revealed that the HT2 5 min sample

performed most poorly, while the HT2 15 min and HT2 30 min performed best. However, RRDE experiments from the second batch of FeNCB catalysts revealed that the HT1 sample performed most poorly, and the HT2 10 min sample performed best. But in addition to these discrepancies between sample batches, repetition of voltammetry experiments for both the worst and best performing samples from the second batch reveal similar inconsistencies. The following visuals illustrate these results.

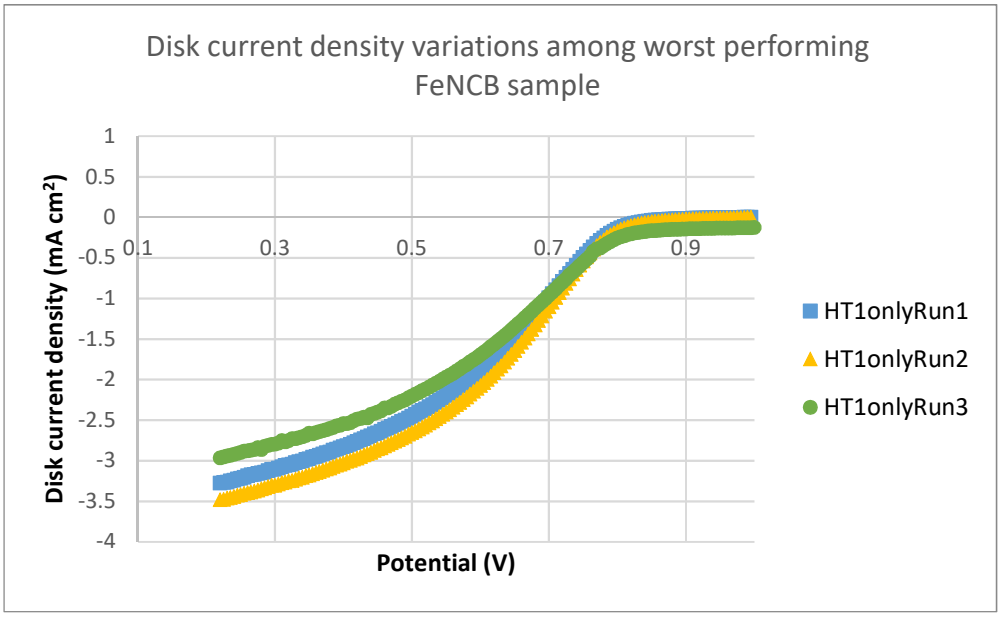

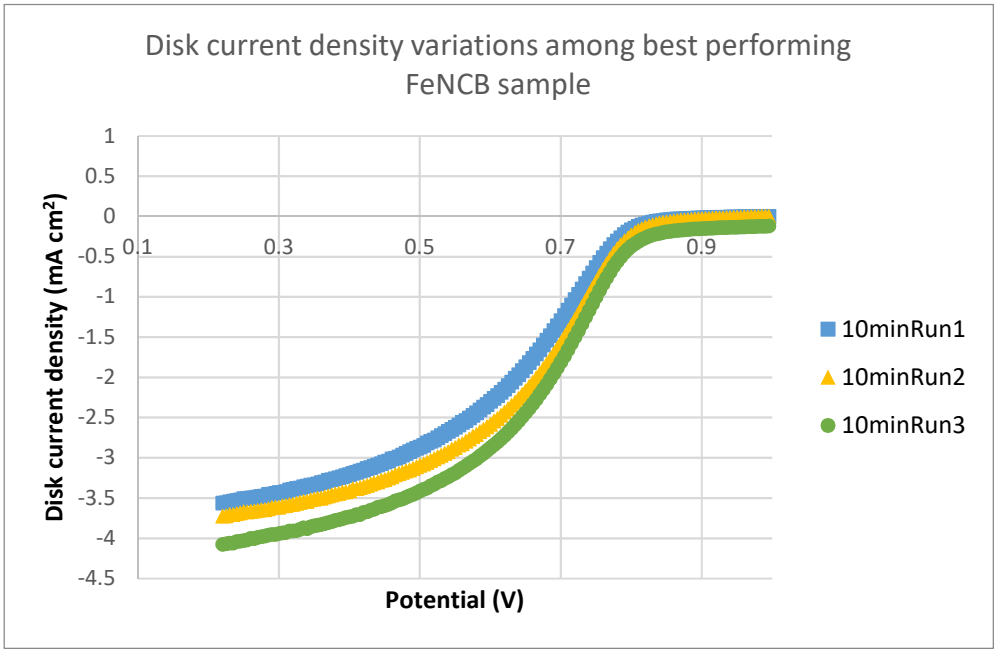

Figure 11: Polarization curves from three RRDE trials performed for the second batch of FeNCB HT1 and FeNCB HT2 10 min samples.

To better quantify the error present here, Table 2 below displays the $E_{1/2}$ values calculated from the above polarization curves as well as those calculated for the three other samples from the second batch.

Sample	Run 1 $E_{1/2}$ (mV)	Run 2 $E_{1/2}$ (mV)	Run 3 $E_{1/2}$ (mV)	Average $E_{1/2}$ (mV)	Standard deviation (mV)
HT1	720	720	730	723.3	4.7
HT2 5 min	725	730	720	725	4.1
HT2 10 min	745	740	730	738.3	6.2
HT2 15 min	745	730	725	733.3	8.5
HT2 30 min	730	730	730	730	0

Table 2: Half-wave potentials for samples synthesized in the second batch of FeNCB catalysts. For each sample, three inks were prepared and tested the same day of preparation. The average half-wave potential and standard deviation was calculated as error measurement.

Here, the issue of irreproducibility is most clearly perceived as the magnitude of standard deviation among $E_{1/2}$ values for one sample sometimes exceeds the difference between $E_{1/2}$ values of different samples, indicating a large amount of error. Despite significant performance deviations in catalysts synthesized in the first and second batch, independent examination of material composition reveals consistency among chemical evolution of nitrogen species from batch to batch.

Section 5: XPS data from second batch of FeNCB samples

One of the major observations from APXPS and XPS analysis of the first batch of FeNCB catalysts was a decrease in pyrrolic nitrogen and an increase in pyridinic nitrogen

after a second pyrolysis was performed. Indeed, high resolution spectra from XPS analysis of a second batch of FeNCB catalysts corroborate these findings.

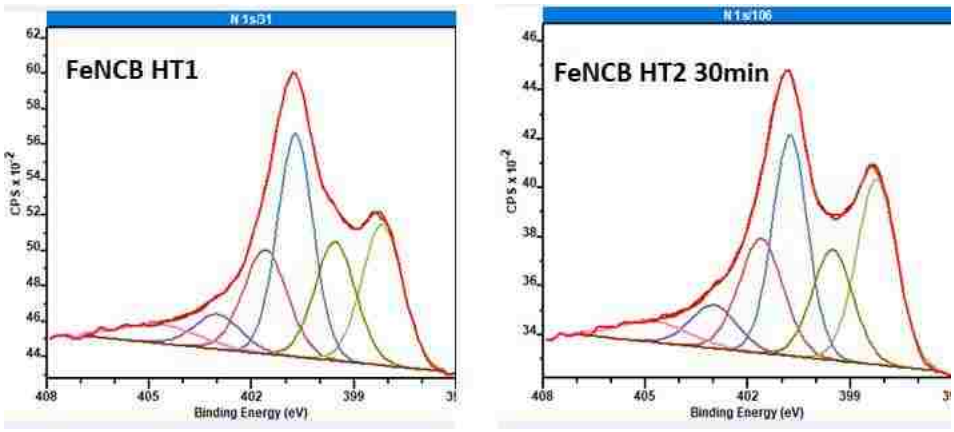

Figure 12: High resolution N 1s XPS spectra for the FeNCB HT1 and FeNCB HT2 30min samples.

Again, after a sample is subjected to the second pyrolysis, there is a distinct increase in signal count at a binding energy of about 398 eV, indicating more binding of pyridinic nitrogen. Another look at the compositional changes over the time of the second pyrolysis produces very similar trends to those observed for the first batch of FeNCB catalysts.

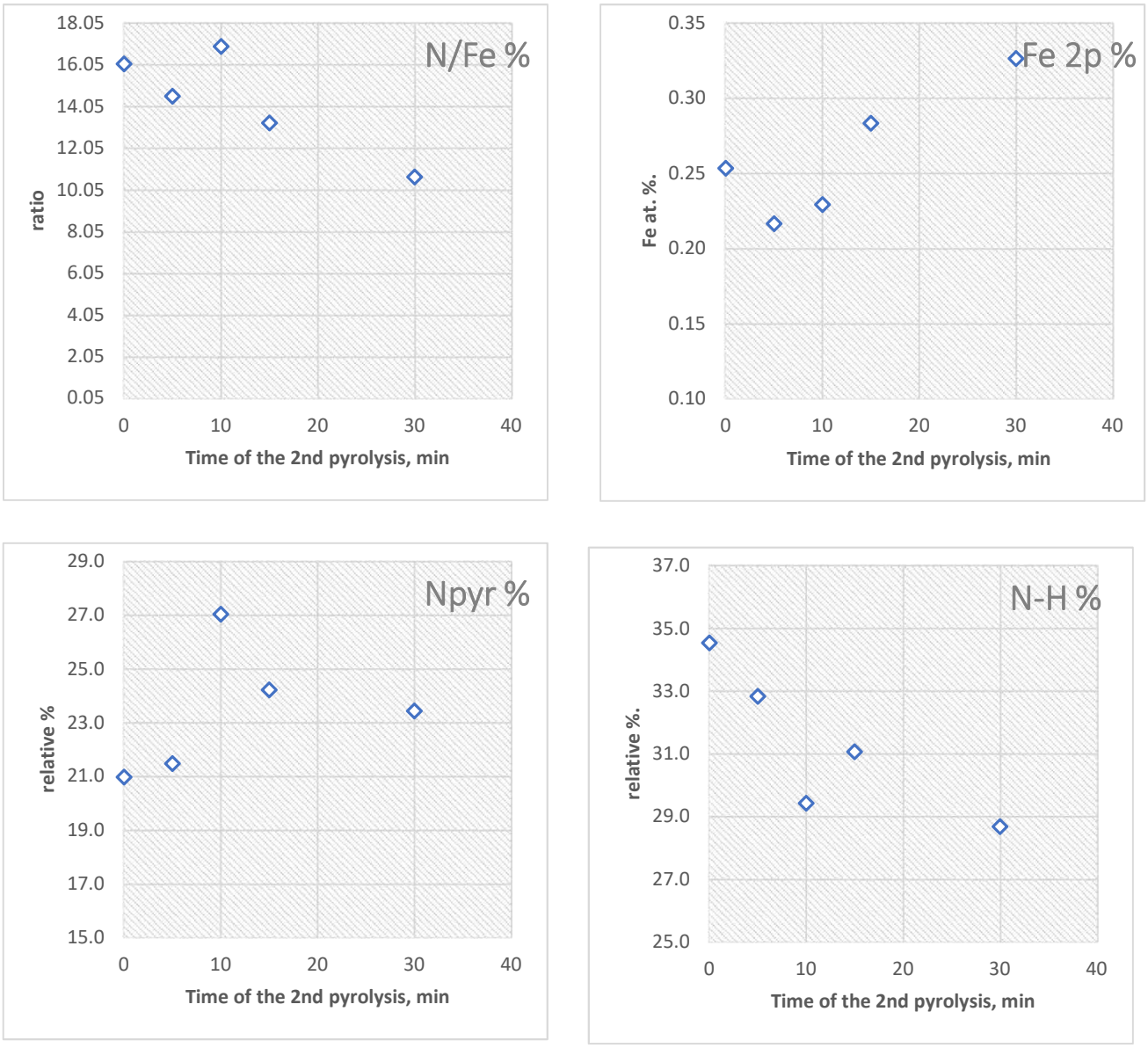

Figure 13: Compositional XPS data for second batch of FeNCB samples

While XPS data of the second FeNCB batch contains more outlier points than data from the first batch, once again the atomic percentage of iron increases over the time of the second pyrolysis thereby decreasing the nitrogen to iron ratio. Furthermore, as the second pyrolysis proceeds a larger portion of nitrogen is found as pyridinic nitrogen than protonated nitrogen. The depiction below compares the structures of pyridinic nitrogen

and pyrrolic nitrogen to show why trends for protonated nitrogen are shown here instead of pyrrolic nitrogen, as evaluation of either species could reveal the same information.

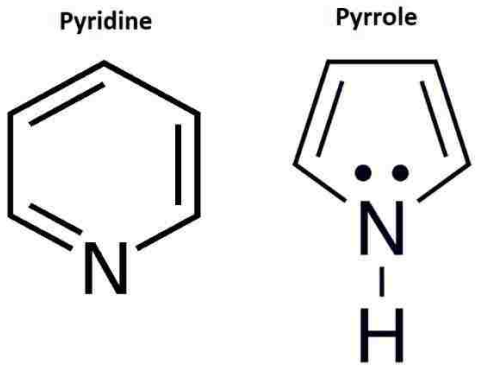

Figure 14: Comparison of the structures of a pyridine and pyrrole

Since the defining difference between pyridinic and pyrrolic nitrogen is the loss of the double bond to protonation, an investigation into the changes of protonated nitrogen was done simply to see if the same trend previously observed for pyrrolic nitrogen would be reciprocated, which it was. Given these patterns in chemistry, a number of conclusions can be drawn as to how the structure of FeNCB catalysts changes over the course of a second pyrolysis treatment.

Conclusions and Future Work

Section 1: Summary of results

This study aimed to fulfill two main objectives, the first being to determine how nitrogen chemistry evolves over the course of the second pyrolysis as well as how morphology changes with time of the second pyrolysis. APXPS and XPS analysis revealed that for two independently synthesized batches of FeNCB catalysts, binding of pyridinic nitrogen species increased, pyrrolic nitrogen binding decreased, and nitrogen to

metal binding increased over the course of a 30-minute secondary pyrolysis. As for morphology, SEM and digital image processing methods evidenced that FeNCB catalysts become more heterogenous over the course of the secondary pyrolysis and the amount of pores between 18 and 80 nanometers in the material increases while the amount of pores between 400 to 600 nanometers in size decreases with increasing time of the second pyrolysis.

The second goal of this study was find some sort of link between catalyst composition and performance when the time of secondary pyrolysis was varied. Figure 15 below shows $E_{1/2}$ values from RRDE experiments of the second batch of catalysts as a function of catalyst content of different types of nitrogen species as evaluated through the XPS data shown in this work.

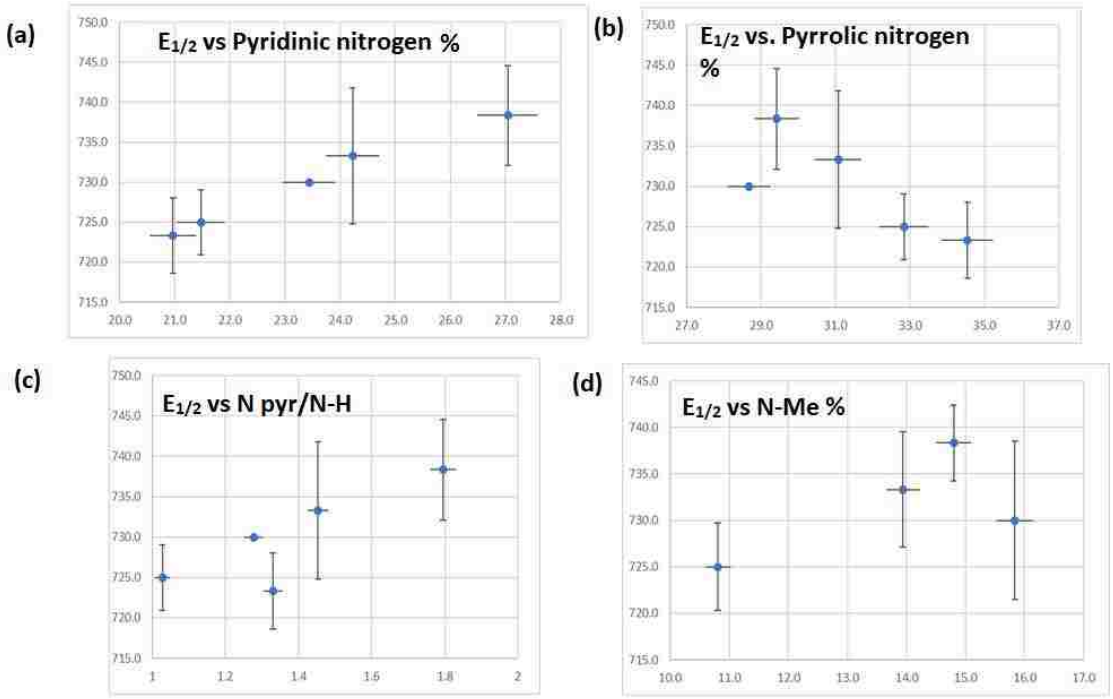

Figure 15: (a) Half-wave potentials from RRDE analysis of second batch FeNCB catalysts as a function of relative pyridinic nitrogen content. (b) Half-wave potentials

from RRDE analysis of second batch FeNCB catalysts as a function of relative pyrrolic nitrogen content. (c) Half-wave potentials from RRDE analysis of second batch FeNCB catalysts as a function of pyridinic nitrogen to protonated nitrogen content ratios (d) Half-wave potentials from RRDE analysis of second batch FeNCB catalysts as a function of the relative percent of nitrogen bound to metal.

Due to significant issues with irreproducibility of RRDE performance data in this study, it cannot be said how the time of second pyrolysis directly affects catalyst performance. For example, this study does not evidence that a FeNCB material pyrolyzed for 10 minutes will perform as a better catalyst than a FeNCB material pyrolyzed for 30 minutes. However, based on the data shown in Figure 15, there are clearly some correlations between the chemistries of the FeNCB catalysts with the highest $E_{1/2}$ potentials. As shown in Figure 15a, the highest $E_{1/2}$ value coincides with the highest pyridinic nitrogen content. The importance of pyridinic nitrogen in catalyst performance is again evidenced in Figure 15c as the highest $E_{1/2}$ value corresponds to the highest ratio of pyridinic nitrogen to hydrogenated nitrogen. Finally, in Figure 15b and 15d, higher $E_{1/2}$ values are seen in regions where pyrrolic nitrogen content is lower and the relative amount of nitrogen bound to metal is higher.

To improve FeNCB catalyst performance, it seems most crucial to increase the contents of pyridinic nitrogen and nitrogen bound to metal of the material. This work has demonstrated that a second high temperature pyrolysis under ammonia can greatly encourage the chemistries of such species beyond the capabilities of just one pyrolysis. However, the time of this secondary pyrolysis is clearly not the point of control for optimizing catalyst performance, so further research is needed to elucidate the mechanisms that can accomplish this.

Section 2: Recommendations for future work

To truly gain insight as to how the second pyrolysis of Fe-NC catalysts improves performance, it would be ideal to observe the evolution of chemical species in real-time as opposed to synthesizing these materials and performing all analyses entirely after the process is completed. Indeed, in situ experiments involving Fe-NC catalysts have been conducted; however, these studies have not been performed during the synthesis of the catalyst, and there is little focus on the evolution of the chemistry of the material[43].

If in situ experimentation is beyond the scope of the non-PGM catalysis field at present time, another worthy approach to elucidate the role of the second pyrolysis in Fe-NC catalyst chemistry and performance is to narrow the focus as to what stage of the process is most relevant. In this study, the majority of the most drastic chemical and morphological changes to catalyst composition and structure occurred during the first five minutes of the second pyrolysis, especially for the first batch of FeNCB catalysts. This highlights a need for research into flash pyrolysis methods. Some studies of this general nature have been published, however in most cases the flash pyrolysis was one of many variables in the synthesis procedure, and there is no consensus of its individual effect[44].

There is also the issue of the rate of heat uptake in how the second pyrolysis determines Fe-NC catalyst properties. If the time duration of the second pyrolysis cannot be shown to play a role in the chemistry behind pyridinic nitrogen or nitrogen to metal binding, then this could be because it is largely dependent on how the sample is intaking energy to break bonds before they can be reconfigured. If a reliable way of measuring sample mass and sample temperature in real-time while the sample is being pyrolyzed could be developed, then this phenomenon could be investigated through caloric energy

transfer. Such advancements in the field could elevate Fe-NC and non-PGM catalysts to the forefront of fuel cell technology and help make sustainable, clean, and cost-effective energy a reality.

References

1. U.S. Energy Facts - Energy Explained, Your Guide To Understanding Energy - Energy Information Administration. Available at: https://www.eia.gov/energyexplained/?page=us_energy_home. (Accessed: 4th November 2017)
2. The Hidden Costs of Fossil Fuels. *Union of Concerned Scientists* Available at: http://www.ucsusa.org/clean-energy/coal-and-other-fossil-fuels/hidden-cost-of-fossils. (Accessed: 4th November 2017)
3. Report Examines Hidden Costs of Energy Production and Use. Available at: http://www8.nationalacademies.org/onpinews/newsitem.aspx?RecordID=12794. (Accessed: 4th November 2017)
4. Survey, I. M. F. IMF Survey : Counting the Cost of Energy Subsidies. *IMF* Available at: http://www.imf.org/en/News/Articles/2015/09/28/04/53/sonew070215a. (Accessed: 4th November 2017)
5. IMF: 'True cost' of fossil fuels is $5.3 trillion a year. *Public Radio International* Available at: https://www.pri.org/stories/2015-06-07/imf-true-cost-fossil-fuels-53-trillion-year. (Accessed: 4th November 2017)
6. How long before we run out of fossil fuels? *Our World in Data* (2017).
7. American energy use up slightly, carbon emissions almost unchanged. *Lawrence Livermore National Laboratory* (2015). Available at: https://www.llnl.gov/news/american-energy-use-slightly-carbon-emissions-almost-unchanged-0. (Accessed: 4th November 2017)

8. U.S. Electric Vehicle Sales Soared In 2016. Available at: https://www.forbes.com/sites/rrapier/2017/02/05/u-s-electric-vehicle-sales-soared-in-2016/#254c8d3217f1. (Accessed: 3rd April 2018)
9. A Basic Overview of Fuel Cell Technology. Available at: http://americanhistory.si.edu/fuelcells/basics.htm. (Accessed: 6th November 2017)
10. Workman, Michael. A study of iron-nitrogen-carbon fuel cell catalysts: chemistry-nanostructure-performance. (University of New Mexico, 2017).
11. Wang, Yun., Chen, Ken., Mishler, Jeffrey., Cho, Sung Chan. & Adroher, Xavier Cordobes. A review of polymer electrolyte membrane fuel cells: Technology, applications, and needs on fundamental research. *Applied Energy* **88,** 981–1007 (2011).
12. Fuel Cell Vehicles - Benefits and Challenges. Available at: https://www.fueleconomy.gov/feg/fcv_benefits.shtml. (Accessed: 5th November 2017)
13. Types of Fuel Cells | Department of Energy. Available at: https://energy.gov/eere/fuelcells/types-fuel-cells. (Accessed: 7th November 2017)
14. Mehta, Viral & Cooper, Joyce Smith. Review and analysis of PEM fuel cell design and manufacturing. *Journal of Power Sources* **114,** 32–53 (2003).
15. Commodities: Latest Platinum Price & Chart. *NASDAQ.com* Available at: https://www.nasdaq.com/markets/platinum.aspx. (Accessed: 27th March 2018)
16. Proietti, Eric., Jaouen, Frédéric., Lefèvre, Michael., Larouche, Nicholas., Tian, Juan., Herranz, Juan., Dodelet, Jean-Pol. Iron-based cathode catalyst with enhanced power

density in polymer electrolyte membrane fuel cells. *Nature Communications.* **2,** 416 (2011).

17. Colgan, J. D. Oil, Conflict, and U.S. National Interests | Belfer Center for Science and International Affairs. (2013). Available at: https://www.belfercenter.org/publication/oil-conflict-and-us-national-interests. (Accessed: 28th March 2018)
18. Lefton, Rebecca & Weiss, Daniel. J. Oil Dependence Is a Dangerous Habit. *Center for American Progress*
19. Lillie, Alain & Lowenkroan, Gabe. OIL & WAR:A NEW DIMENSION TO INTERNATIONAL SECURITY. Available at: https://web.stanford.edu/class/e297c/trade_environment/energy/hoil.html. (Accessed: 28th March 2018)
20. Jasinski, Raymond. A New Fuel Cell Cathode Catalyst. *Nature* **201,** 1212–1213 (1964).
21. Ghosh, Abhik. *The Smallest Biomolecules: Diatomics and their Interactions with Heme Proteins*. (Elsevier, 2011).
22. Liu, Jing., Li, Erling., Ruan, Mingbo., Song, Ping. & Xu, Weilin. Recent Progress on Fe/N/C Electrocatalysts for the Oxygen Reduction Reaction in Fuel Cells. *Catalysts* **5,** 1167–1192 (2015).
23. Song, Chaojie. & Zhang, Jiujun. *PEM Fuel Cell Electrocatalysts and Catalyst Layers*. (2008).
24. Power density - Energy Education. Available at: http://energyeducation.ca/encyclopedia/Power_density. (Accessed: 30th March 2018)

25. Zagal, Jose H. & Bedioui, Fethi. *Electrochemistry of N4 Macrocyclic Metal Complexes*. **1,** (2016).

26. Monk, Paul M. S. *Fundamentals of Electroanalytial Chemistry*. (John Wiley & Sons, 2008).

27. Serov, Alexey., Artyushkova, Kateryna., Niangar, Ellazar., Wang, Chunmei., Dale, Nilesh., Jaouen, Frederic., Sougrati, Moulay-Tahar., Jia, Qingying., Mukerjee, Sanjeev., Atanassov, Plamen. Nano-structured non-platinum catalysts for automotive fuel cell application. *Nano Energy* **16,** 293–300 (2015).

28. Durability Working Group | Department of Energy. Available at: https://www.energy.gov/eere/fuelcells/durability-working-group. (Accessed: 31st March 2018)

29. Gu, Lingzheng., Jiang, Luhua., Li, Xuning., Jin, Jutao., Wang, Junhu., Sun, Gongquan. A Fe-N-C catalyst with highly dispersed iron in carbon for oxygen reduction reaction and its application in direct methanol fuel cells. *Chinese Journal of Catalysis.* **37,** 539–548 (2016).

30. Wang, Qiang. *et al.* Phenylenediamine-Based FeNx/C Catalyst with High Activity for Oxygen Reduction in Acid Medium and Its Active-Site Probing. *Journal of the American Chemical Society.* **136,** 10882–10885 (2014).

31. Kramm, Ulrike. I., Herrmann-Geppert, Iris., Bogdanoff, Peter. & Fiechter, Sebastian. Effect of an Ammonia Treatment on Structure, Composition, and Oxygen Reduction Reaction Activity of Fe–N–C Catalysts. *Journal of Physical Chemistry. C* **115,** 23417–23427 (2011).

32. Workman, Michael. J. *et al.* Platinum group metal-free electrocatalysts: Effects of synthesis on structure and performance in proton-exchange membrane fuel cell cathodes. *Journal of Power Sources* **348,** 30–39 (2017).
33. Liu, Gang., Li, Xuguang., Ganesan, Prabhu. & Popov, Branko. N. Studies of oxygen reduction reaction active sites and stability of nitrogen-modified carbon composite catalysts for PEM fuel cells. *Electrochimica Acta* **55,** 2853–2858 (2010).
34. Artyushkova, Kateryna., Matanovic, Ivana., Halevi, Barr. & Atanassov, Plamen. Oxygen Binding to Active Sites of Fe-N-C ORR Electrocatalysts Observed by Ambient-Pressure XPS. *Journal of Physical Chemistry.*
35. Herranz, Juan. *et al.* Unveiling N-Protonation and Anion-Binding Effects on Fe/N/C Catalysts for O2 Reduction in Proton-Exchange-Membrane Fuel Cells. *Journal of Physical Chemistry. C* **115,** 16087–16097 (2011).
36. Structure-to-property relationships in fuel cell catalyst supports: Correlation of surface chemistry and morphology with oxidation resistance of carbon blacks - ScienceDirect. Available at: https://www.sciencedirect.com/science/article/pii/S0378775312008294. (Accessed: 4th April 2018)
37. Artyushkova, Kateryna. *GUI for calculating 1st and 2nd order statistics from images*.
38. Knudsen, Jan., Andersen, Jesper. N. & Schnadt, Joachim. A versatile instrument for ambient pressure x-ray photoelectron spectroscopy: The Lund cell approach. *Surface Science.* **646,** 160–169 (2016).
39. Kelemen, Simon. R., Gorbaty, Martin. L. & Kwiatek, Peter. J. Quantification of Nitrogen Forms in Coals. *Energeia* **6,** (1995).

40. Nie, Yao., Li, Li. & Wei, Zidong. Recent advancements in Pt and Pt-free catalysts for oxygen reduction reaction. *Chemical Society Reviews* **44,** 2168–2201 (2015).
41. Cha, Chuansin S., Shao, Meijun J. & Liu, Chungchiun C. Problems associated with the miniaturization of a voltammetric oxygen sensor: Chemical crosstalk among electrodes. *Sensors and Actuators B Chemistry.* **2,** 239–242 (1990).
42. Van Den Brink, F., Visscher, W. & Barendrecht, Embrecht. Electrocatalysis of cathodic oxygen reduction by metal phthalocyanines: Part III. Iron phthalocyanine as electrocatalyst: experimental part. *J. Electroanalytical Chemistry and Interfacial Electrochemistry.* **172,** 301–325 (1984).
43. Malko, Daniel, Kucernak, Anthony & Lopes, Thiago. In situ electrochemical quantification of active sites in Fe–N/C non-precious metal catalysts. *Nature Communications.* **7,** 13285 (2016).
44. A General Approach to Preferential Formation of Active Fe–Nx Sites in Fe–N/C Electrocatalysts for Efficient Oxygen Reduction Reaction - Journal of the American Chemical Society (ACS Publications). Available at: https://pubs.acs.org/doi/abs/10.1021/jacs.6b09470. (Accessed: 8th April 2018)